Effect of the DC link Parameters on Transient Peaks and Harmonics Generated due to Grid Faults in Wind-Driven DFIG

MONA N. ESKANDER, SANAA M.I. AMER
Power Electronics and Energy Conversion Dept.
Electronics Research Institute
Cairo, EGYPT

Abstract :- In this paper, the effect of the DC link capacitor (C_d), and DC link inductor (L_d), on the performance of the grid-connected, wind-driven, Double-Fed Induction generator (DFIG) is investigated during 3-phase symmetrical grid-voltage faults. The DFIG system is modelled using Matlab/Simulink software, and simulation results are plotted against C_d and L_d for each of the three considered grid faults. The transient peaks of the stator current, rotor current, rotor voltage, and DC link current and voltage, due to grid voltage sag, grid voltage swell, and the 3-phase-to-ground fault at different values of C_d and L_d are presented. The current and voltage harmonics generated due to grid faults at different C_d and L_d values are also investigated. The time taken by the DFIG currents and voltages to reach their steady state is calculated, for the 3-phase ground fault, as a function of DC link parameters. Investigating the responses of stator and rotor currents, rotor voltage, and DC-link voltage and current at different values of C_d and L_d lead to conclude the optimum values of the DC-link parameters that lead to fast fault recovery.

Key-Words :- Double-Fed Induction generator (DFIG), DC link capacitor (C_d), DC link inductor (L_d), 3-phase symmetrical grid-voltage faults

Received: April 19, 2024. Revised: November 11, 2024. Accepted: December 13, 2024. Published: March 21, 2025.

1 Introduction

Wind energy is a clean and affordable power source that has seen a significant increase in installations over the past two decades [1-3]. Conventional stall wind turbines are equipped with cage rotor induction generators, in which the speed is almost constant, while variable-speed wind turbines use doubly-fed induction generators or synchronous generators in connection with partial-rate or full-rate power converters [4-5]. The variable speed wind turbine is able to achieve maximum power coefficient over a wide range of wind speeds and about 5-10 % gain in the energy capture can be obtained.

Doubly-fed induction generator-based wind turbines (DFIG-WTs) are commonly used for variable-speed wind-power generation. These turbines offer advantages such as low cost, low power loss and independent control of active and reactive power.

The DFIG stator is directly connected to the power grid, and the rotor is linked to the power grid through back-to-back converter. The back-to-back converter consists a rotor-side converter (RSC) and a grid-side converter (GSC). The DFIG-WTs is widely popular because only a partially rated wind energy conversion system that is about 25–30% of the system rating is employed [6], leading to a higher efficiency and lower converter cost.

However, because the stator windings are directly connected to the grid, DFIG-WTGs are sensitive to grid disturbances, such as voltage sags, voltage swells, or ground faults. With the rapidly increased penetration of wind power and concentrated wind power installation, disconnection of WTGs due to voltage disturbances can cause serious problems on the power system stability [7]. Modern grid codes require wind turbines to stay connected to the grid during transients and severe faults. Hence rapid detection and mitigation of the effect of these faults ensures the continuous connection of the DFIG-WT system.

To address this issue, various protection circuits and control methods have been explored to enhance the fault-ride-through (FRT) capability of DFIG-WTs [8-15]. In [8], a computing technique is proposed to detect the grid- voltage fluctuation. In [9] a sliding mode control technique is proposed for FRT. In [10] superconducting converter is proposed to enhance FRT. In [11] the FRT is enhanced through a non-linear controller, while in [12] finite space model predictive command is proposed to manage wind farms to improve the quality of the current output from the DFIG with considering fault ride through technique. In [13] an event-triggered sliding mode control (ETSMC) is combined with a super-capacitor and a high-frequency magnetic-linked dual active bridge converter for FRT. A STATCOM is applied for FRT in [14].

The DC-link voltage is generally controlled to be constant during both normal [15] and abnormal situations. Hence, to control the DC-link voltage and protect the switches of the back-to-back converters from over-current damage due to grid faults, the influence of the DC-link capacitor and inductor has to be extensively investigated.

In this paper, the influence of the DC link capacitor C_d, and DC link inductor L_d, on the performance of the DFIG-WT during grid voltage sag, grid voltage swell, and 3-phase ground fault is investigated. Modeling the DFIG-WT system is done using Matlab/Simulink software, and simulation results are plotted versus C_d and L_d for each of the three considered grid faults. The simulation results include variation of the transient peaks of stator current, rotor current, rotor voltage, DC link current, and DC link voltage versus C_d at constant L_d, and then versus L_d at constant C_d. Also, the DFIG current and voltage harmonics generated due to grid faults at different C_d and L_d values are presented. The time taken by each DFIG variable to reach its steady state is plotted as a function of the DC link parameters. Investigating the transient peaks of stator and rotor currents, rotor voltage, and DC-link voltage and current versus values of C_d and L_d leads to conclude the optimum values of the DC-link parameters that lead to fast fault recovery.

Results proved the drastic effect of the DC link capacitor (C_d) on the transient peaks of the DFIG AC and DC variables and on the time taken to reach their steady values after the grid voltage sags, swells, and ground faults. The THD of stator and rotor currents and rotor voltages are also affected by the DC link capacitor. Similarly, the results showed the tangible effect of varying the DC link inductor L_d at constant C_d on the current and voltage transient peaks after grid faults, and on the voltage and current harmonics. The DC parameters (C_d and L_d) that lead to faster recovery from grid faults, and lower current and voltage harmonics, are hence deduced.

The main contributions in this research paper are summarized as follows:

1-Examining the effect of the DC link inductor as well as the DC link capacitor on the DFIG response to grid faults, while previous work concentrated mainly on the DC link capacitor.

2- Demonstrating the time that elapsed till the stator and rotor currents and the rotor voltage regained their steady state value, after the grid faults, as a function of DC link parameters.

3-Investigating the effect of the DC link parameters on the harmonics injected into the grid aids in improving the power quality.

2 System Modeling

The following mathematical models illustrate how the DFIG-WT system, shown in Fig. 1, behaves under three types of grid faults.

2.1 Turbine model

Wind turbine output power *Pw* is given by:

$$P_w = 0.5\, C_p(\lambda\,, \beta)\rho\pi R^2\, V_w \tag{1}$$

where *Vw* is the wind speed, ρ is the air density, *R* is the radius of the wind turbine, *Cp* is the wind turbine power coefficient, λ is the tip-speed ratio, and β is the pitch angle.

The aerodynamic power coefficient C_p is a function of the tip speed ratio, λ, and the pitch angle, β, as follows [16]:

$$C_p(\lambda\,, \beta) = 0.22\,\left(\frac{116}{\lambda_1} - 0.4\beta - 5\right) e^{\frac{12.5}{\lambda_1}} \tag{2}$$

$$\lambda = \frac{R\omega_w}{V_w} \tag{3}$$

Where ω_w is the angular rotor

2.2 Induction machine model

The DFIG, shown in Fig. (1), is a wound-rotor induction machine in which the stator is directly connected to the grid and the rotor is connected to the grid through back-to-back power converters.

The DFIG dynamical equations in the d-q synchronously rotating frame are given as follows [17]:

$$\frac{d\varphi_{ds}}{dt} = v_{ds} - r_s\, i_{ds} + w\varphi_{qs} \tag{4}$$

$$\frac{d\varphi_{qs}}{dt} = v_{qs} - r_s\, i_{qs} + w\varphi_{ds} \tag{5}$$

$$\frac{d\varphi_{dr}}{dt} = v_{dr} - r_r\, i_{dr} + (w - w_r)\,\varphi_{qr} \tag{6}$$

$$\frac{d\varphi_{qr}}{dt} = v_{qr} - r_r\, i_{qr} - (w - w_r)\,\varphi_{dr} \tag{7}$$

$$\frac{dw_r}{dt} = \frac{1}{2H}\,(T_e - T_L - B_m w_r) \tag{8}$$

$$\varphi_{ds} = L_s i_{ds} + L_m i_{dr} \tag{9}$$

$$\varphi_{qs} = L_s i_{qs} + L_m i_{qr} \tag{10}$$

$$\varphi_{dr} = L_r i_{dr} + L_m i_{ds} \tag{11}$$

$$\varphi_{qr} = L_r i_{qr} + L_m i_{qs} \quad (12)$$

$$Te = \frac{3PL_m}{4\,L_s}\left(\varphi_{qs}\,i_{dr} - \varphi_{ds}\,i_{qr}\right) \quad (13)$$

$$T_m - T_e = 2H\frac{d\omega_r}{dt} \quad (14)$$

The active power and reactive are given by:

$$P = V_{ds}i_{ds} + V_{qs}i_{qs} + V_{dr}i_{qr} + V_{qr}i_{qr} \quad (15)$$

$$Q = V_{qs}i_{ds} - V_{ds}i_{qs} + V_{qr}i_{dr} - V_{dr}i_{qr} \quad (16)$$

Where …φ, v, i, ω, T_e, T_m, H, r, and L, denote flux, voltage, current, angular speed, electromagnetic torque, mechanical torque, inertia constant, resistance and inductance respectively.

Subscripts d and q denote d-axis and q-axis components in synchronously d-q reference frame.
Subscripts s, r, and m denote stator, rotor, and mutual quantities respectively;
P is the number of pole pairs

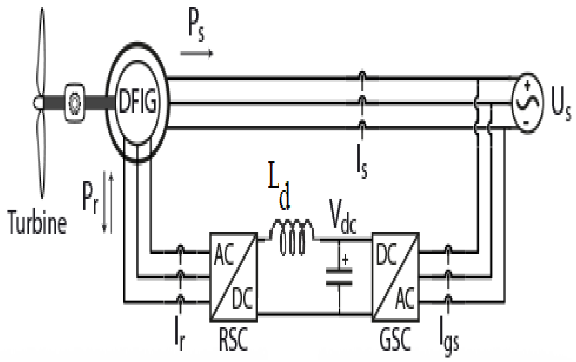

Fig. 1: The wind-driven grid-connected DFIG

2.3 Back-to-back converter

The two voltage-source back-to-back converters model in the rotating reference frame d-q is given by

$$\mathrm{L}\dot{\mathrm{i}}_{\mathrm{d}} = -\mathrm{r}\mathrm{i}_{\mathrm{d}} - \mathrm{L}\omega\mathrm{i}_{\mathrm{q}} + \eta\mathrm{v}_{\mathrm{dc}} - \mathrm{v}_{\mathrm{d}} \quad (17)$$

$$\mathrm{L}\dot{\mathrm{i}}_{\mathrm{q}} = -\mathrm{r}\mathrm{i}_{\mathrm{q}} + \mathrm{L}\omega\mathrm{i}_{\mathrm{d}} + \eta_{\mathrm{q}}\mathrm{v}_{\mathrm{dc}} - \mathrm{v}_{\mathrm{q}} \quad (18)$$

$$C_{dc}\dot{\mathrm{v}}_{\mathrm{dc}} = -(1.5)\left(\eta i_d + \eta_q i_q\right) + \mathrm{i}_{\mathrm{l}} \quad (19)$$

Where η is the control signal, and subscripts dc stand for dc link variables.

2.4 The DC link parameters L_d and C_d

The RSC is susceptible to AC ripples. The switching frequency produces ripples above 500 kHz, which are often coupled to the output voltage. The DC link inductor L_d, shown in Fig.1, opposes a fast change in current, thereby giving a smoother DC output. This is backed up by the capacitor C_d at the output side of the inductor in parallel with GSI. This stabilizes the voltage still further.

Choosing a value for L_d, the capacitor can be calculated from the resonance frequency

$$f=0.5/\sqrt{L_d C_d} \quad (20)$$

3 Simulation Results at Constant L_d

The Matlab-Simulink software is used to model and simulate the DFIG-WT system. This section presents simulation results with fixed L_d under three different types of grid faults.

3.1 Influence of DC link capacitor on DFIG performance during 3-phase voltage sag

A 3-phase symmetrical grid voltage sag of 70% from the rated grid voltage is assumed at t= 0.3 second for 0.2 seconds. Figure 2 demonstrates stator and rotor voltages and currents during voltage sag.

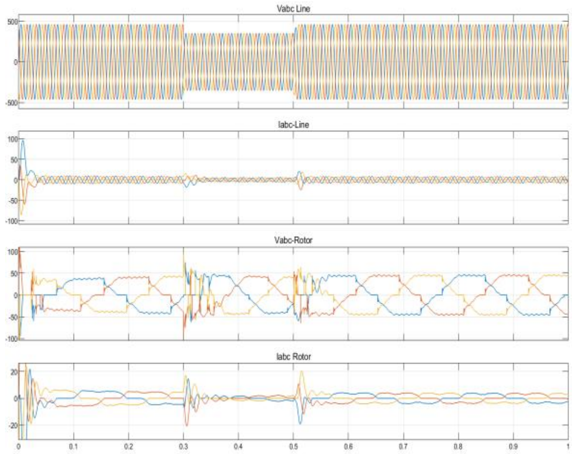

Fig 2 Stator and rotor voltages and currents during voltage sag

The transient peaks of the stator current, the rotor currents, and the rotor voltage, due to the 3-phase grid voltage sag are calculated as a function of the DC link capacitor C_d and plotted in Fig.3. The DC link inductor is maintained at 0.005 H. It is clear that the transient response of these three variables differs. The stator current peak increases with the increase in C_d, while the rotor current reaches its peak value at C_d= 0.5 F and then decreases as C_d increases. The rotor voltage reaches its highest peak at the lowest C_d, and then decreases as C_d increases.

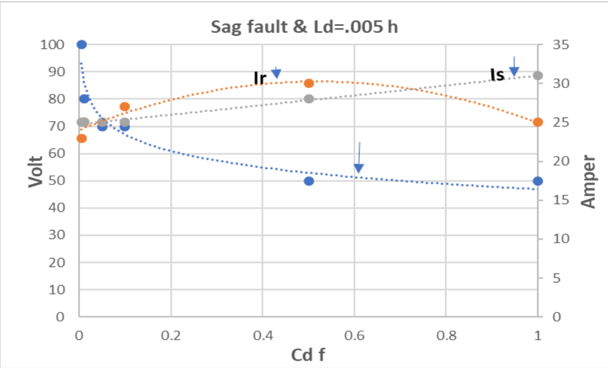

Fig. 3 Transient peaks of stator current, rotor current, & rotor voltage due to voltage sag

Investigating the time taken for the DFIG stator and rotor currents as well as rotor voltage to regain their steady-state values after a grid voltage sag revealed that the time increases as the capacitor size increases. Additionally, the time for the DC link voltage and current to reach a steady state after a voltage sag also increases with an increase in C_d.

3.2 Influence of DC link capacitor on DFIG performance during 3-phase voltage swell

A 3-phase symmetrical grid voltage swell (130%) is assumed at t= 0.3 second for 0.2 seconds. Figure 4 demonstrates stator and rotor voltages and currents during the voltage swell.

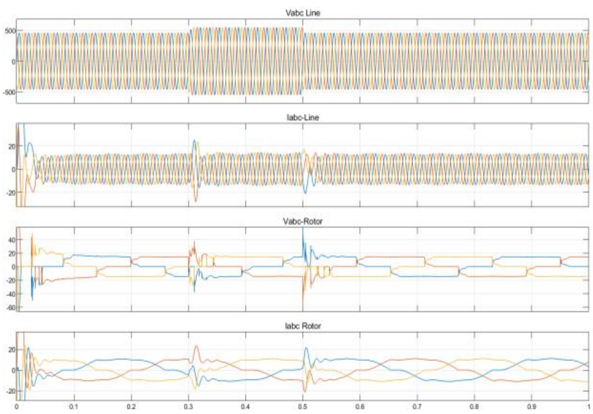

Fig 4 stator and rotor voltages and currents during voltage swell

The transient peaks of the stator current, the rotor currents, and the rotor voltage, due to the 3-phase grid voltage swell are calculated as a function of the DC link capacitor C_d and plotted in Fig.5.The DC link inductor is maintained at 0.005 H. It is clear that the transient response of the three DFIG AC parameters; namely stator current, rotor current, and rotor voltage, are different from each other and from their responses during the grid voltage sag. The stator current transient peak increases with the increase in C_d until 0.5 F and then decreases at higher C_d values. The rotor current transient peak increases as C_d increases. The rotor voltage transient peak reaches its highest value at the lowest C_d, and then decreases as C_d increases.

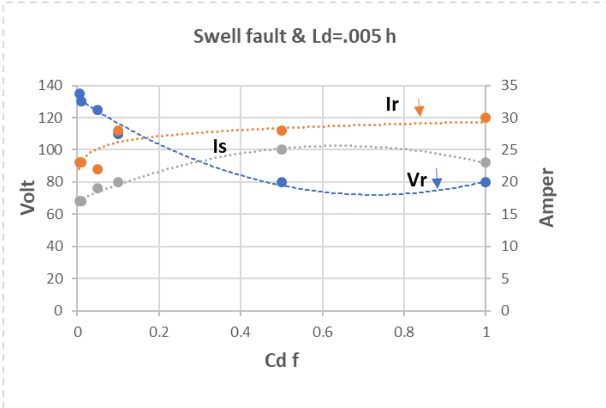

Fig. 5 transient peaks of stator current, rotor current, & rotor voltage due to voltage swell

3.3 Influence of DC link capacitor on DFIG performance during 3-phase ground fault

A 3-phase symmetrical ground fault is assumed at t= 0.3 seconds for 0.2 seconds. Figure 6 demonstrates stator and rotor voltages and currents during the 3-phase ground fault.

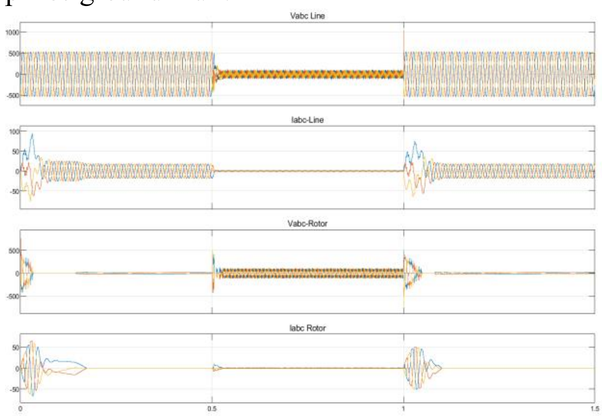

Fig 6 stator and rotor voltages and currents during ground fault

The transient peaks of the stator current, rotor current, and rotor voltage, due to the 3-phase ground fault are calculated as a function of the DC link capacitor C_d and plotted in Fig.7. The DC link inductor is maintained at 0.005 H. The responses of the AC variables differ from those during grid voltage sag and swell. The transient peak of the stator current increase as C_d is increased, while the rotor current reaches its peak value at C_d= 0.5 F and then decreases as C_d increases. The rotor voltage peak reaches its highest value at the lowest C_d, and then decreases as C_d increases.

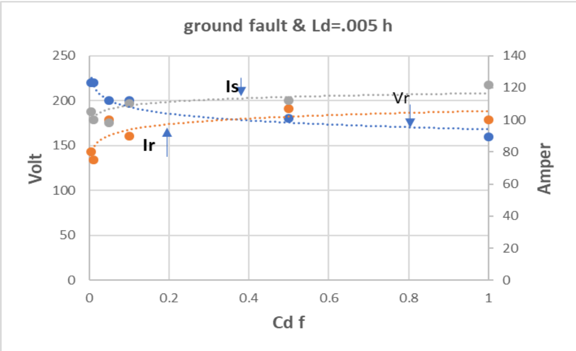

Fig. 7 transient peaks of stator current, rotor current, & rotor voltage due to 3-phase ground fault

3.4 Harmonics due to 3-phase ground fault at fixed L_d

From Figs. 3, 5, and 7, the transient behavior of the stator and rotor currents and the rotor voltage due to the three types of grid faults are similar as C_d is varied. Hence the effect of C_d on the current and voltage harmonics are investigated for the 3-phase ground fault only.

Plotting the Total Harmonic Distortion THD of the stator current at two values of capacitance (C_d), as shown in Figure 8, reveals a noticeable decrease with increasing C_d (from 15.31% at C_d = 0.005 F to 12.62% at C_d = 0.1 F). However, a slight decrease in the THD of the rotor current occurs as C_d increases as shown in Figure 9. The THD of rotor voltage, presented in Figure 10, also shows a significant decrease as C_d increases.

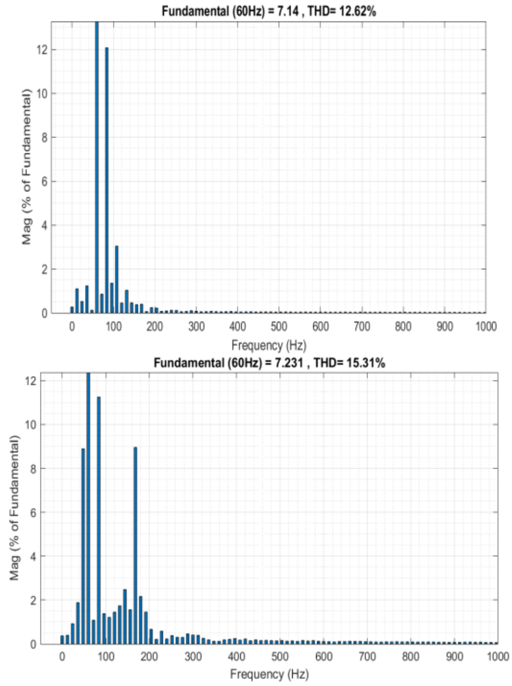

Fig. 8 stator current THD at ground fault

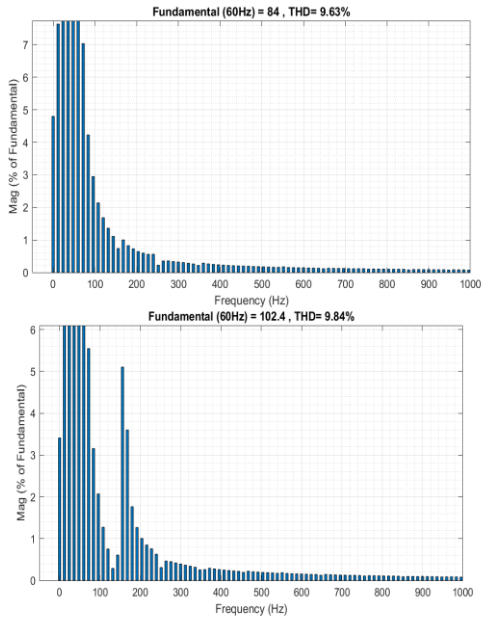

Fig. 9 rotor current THD at ground fault

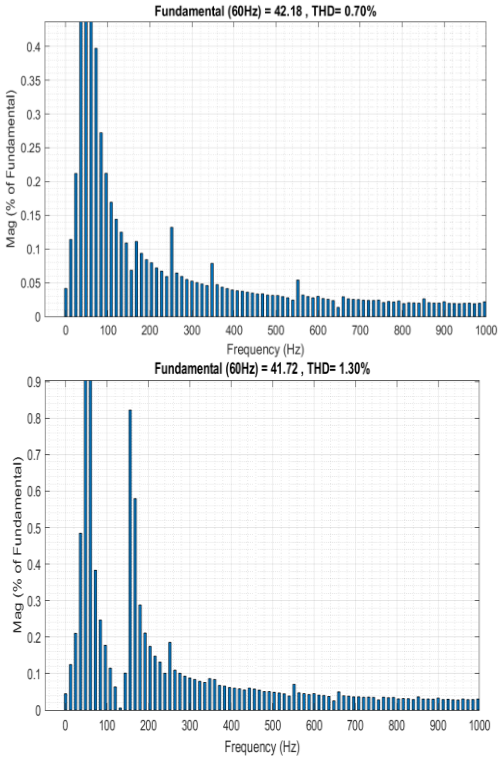

Fig. 10 rotor voltage THD at ground fault

3.5 Settling time due to 3-phase ground fault at fixed L_d

The settling time (Ts) taken by the DC link voltage and current to reach steady state after a ground fault is shown in Figure 11. The same figure, also displays the variation of the peak transients of DC link current and voltage (caused by the ground fault) with C_d. It is observed that the ground fault has a slight impact on the DC link current. The increase in settling time as C_d increases is expected due to the longer capacitor charging time.

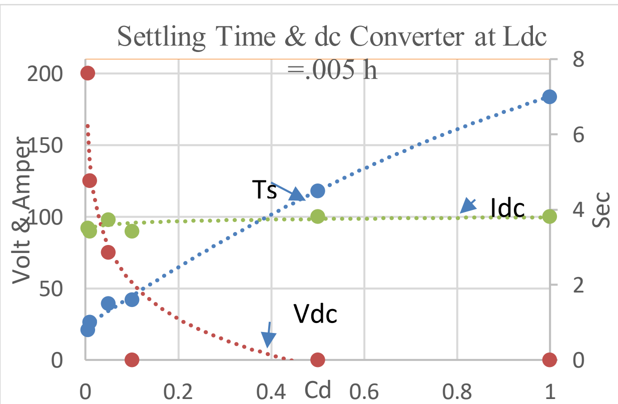

Fig.11 Settling time and DC link variables at 3-phase ground fault at constant L_d

4 Simulation Results at Constant C_d

The Matlab-Simulink software is used to model and simulate the DFIG-WT system. This section presents simulation results with fixed C_d under three different types of grid faults.

4.1 Influence of DC link inductor L_d on DFIG performance during 3-phase voltage sag

A 3-phase symmetrical grid voltage sag of 70% from the rated grid voltage is assumed at t= 0.3 seconds for 0.2 seconds. The transient peaks of the stator current, the rotor currents, and the rotor voltage, due to the 3-phase grid voltage sag are calculated as a function of the DC link inductor L_d and plotted in Fig.12. The DC link capacitor is maintained at 0.1 F. The stator current and the rotor current peaks decrease with the increase of L_d in a similar configuration, while the rotor voltage peak increases with the increase of L_d. It is noticed that the behavior of these variables as L_d varies differs from their behavior as C_d varies.

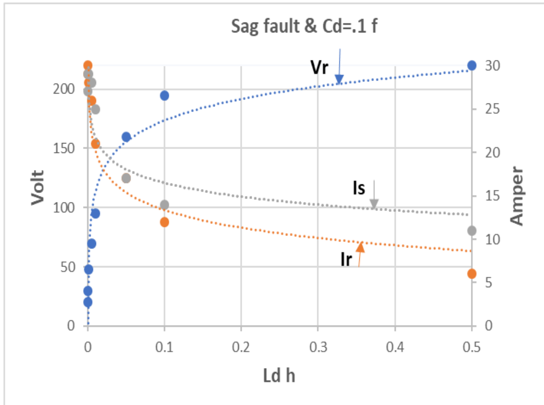

Fig 12 transient peaks of stator current, rotor current, & rotor voltage due to voltage sag at constant C_d

4.2 Influence of DC link inductor L_d on DFIG performance during 3-phase voltage swell

A 3-phase symmetrical grid voltage swell (130 %) is assumed at t= 0.3 second for 0.2 seconds. The transient peaks of the stator current rotor current, and rotor voltage, due to the 3-phase grid voltage swell are calculated as a function of the DC link inductor L_d and plotted in Fig.13. The DC link capacitor is maintained at 0.1 F.

The transient peaks of the stator current and rotor current decrease with an increase in L_d in similar configuration, while the rotor voltage transient peak increases with an increase in L_d. It is noticed that the profiles of these parameters vary similarly to their variation in the case of voltage sag.

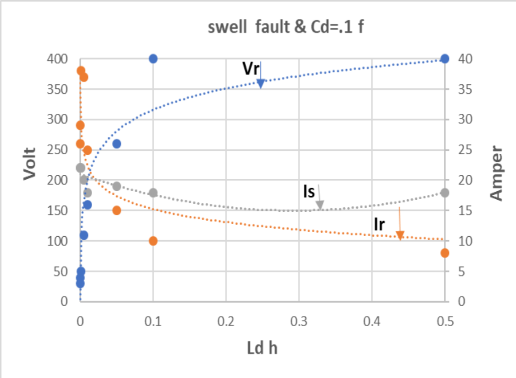

Fig 13 transient peaks of stator current, rotor current, & rotor voltage due to voltage swell at constant C_d

4.3 Influence of DC link inductor on DFIG performance during 3-phase ground fault

A 3-phase symmetrical ground fault is assumed at t= 0.3 second for 0.2 seconds. The transient peaks of stator current, rotor current, and rotor voltage, due to the 3-phase ground fault are calculated as a function of the DC link inductor L_d and plotted in Fig.14. The DC link capacitor is maintained at 0.1F. The transient peaks of stator current and rotor current decrease as L_d is increased, while the rotor voltage peak increases with L_d.

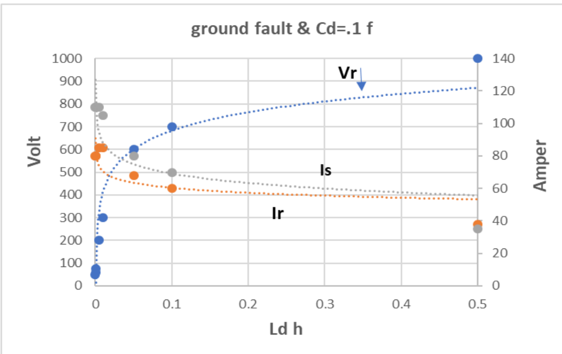

Fig 14 transient peaks of stator current, rotor current, & rotor voltage due to ground fault at constant C_d

The transient behavior of the stator and rotor currents and the rotor voltage due to the three types of grid faults are similar as L_d is varied. Hence the effect of L_d on the current and voltage harmonics are investigated for the 3- phase ground fault only.

4.4 Harmonics due to 3-phase ground fault at fixed C_d

Plotting the total harmonic distortion (THD) of the stator current at two values of L_d, as shown in Fig. 15, reveals a noticeable decrease with increasing L_d (from 13.29% at L_d = 0.0001 H to 10.18% at L_d= 0.05H). However, there is a slight decrease in the THD of the rotor current as L_d increases as shown in Figure 16. The THD of rotor voltage, depicted in Fig.17, also shows a slight decrease as L_d increases.

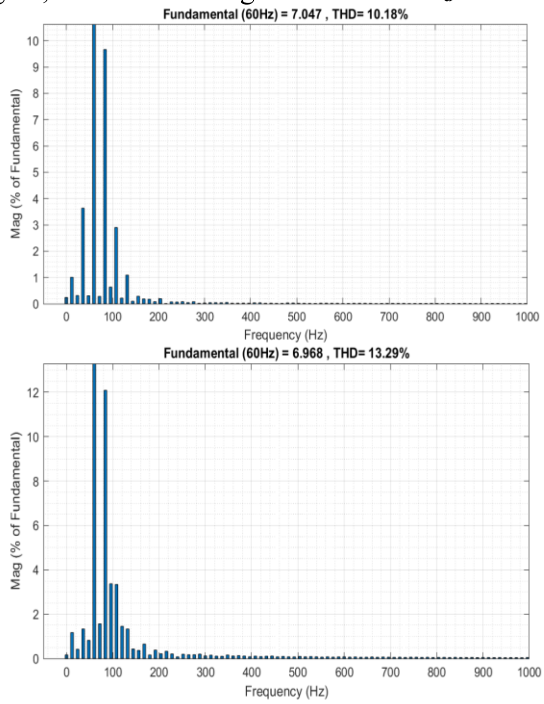

Fig 15 THD of the stator current at two values of L_d

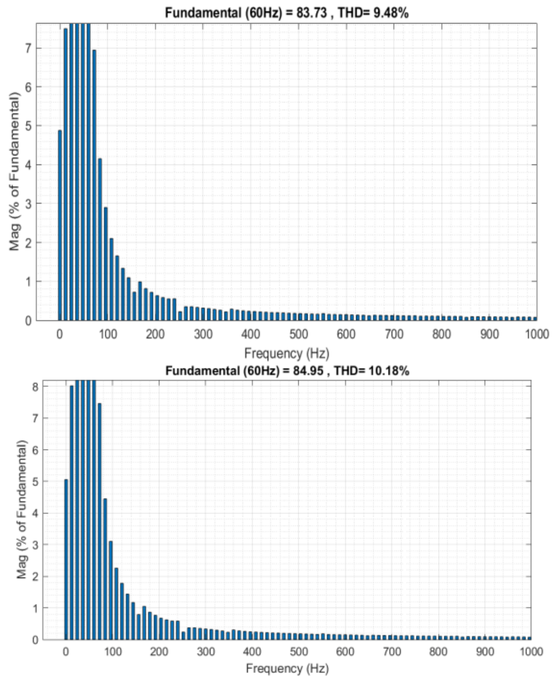

Fig 16 THD of the rotor current at two values of L_d

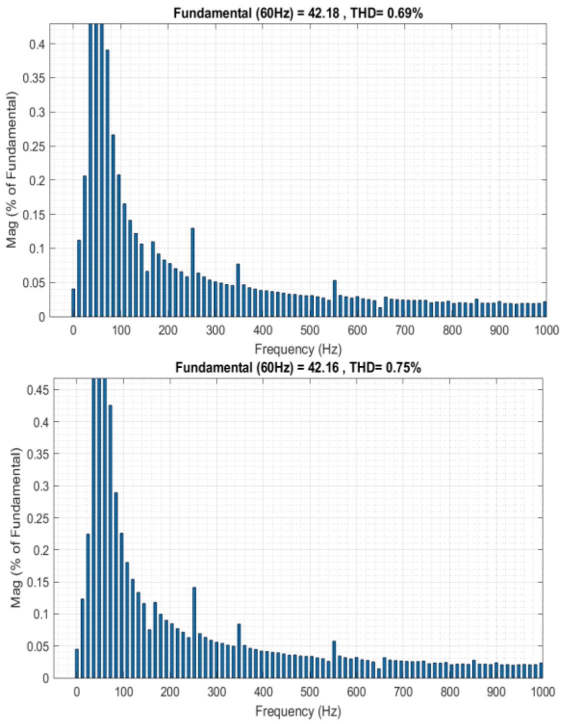

Fig 17 THD of the rotor voltage at two values of L_d

4.5 Settling time due to 3-phase ground fault at fixed C_d

The settling time Ts taken by the DC link voltage and current to reach steady state after a three-phase ground fault is plotted in Fig.18. On the same figure, the variation of the peak transients of DC link current and voltage (due to the ground fault) with L_d are plotted. The increase in settling time Ts as L_d increases is expected due to the increase in time constant. It is worth noting that the settling time for DC link variables is longer when C_d is increased. The peak transient of the DC voltage increases while the peak transient of the current decreases as L_d is increased.

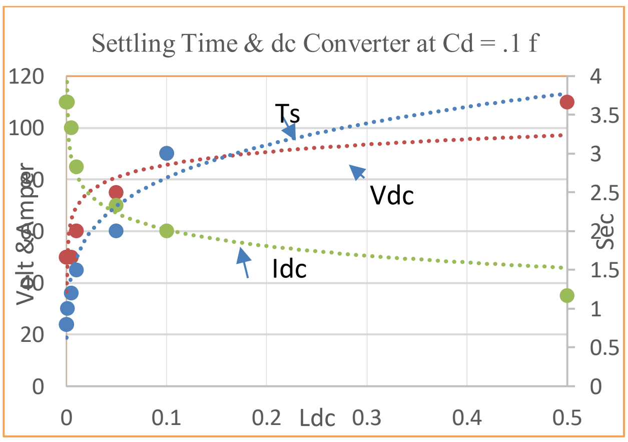

Fig 18 Settling time Ts and DC link variables at constant C_d

5 Conclusion

An investigation of the effect of DC link inductor and capacitor on the transients of a grid connected wind-powered Doubly Fed Induction generator (DFIG) currents and voltages due to three types of grid faults is presented. The proposed faults are; 3-phase voltage sag, 3-phase voltage swell, and 3-phase ground fault. The current and voltage harmonics due to these faults are calculated at different values of inductance (L_d) and capacitance (C_d). The settling time of the DC voltage and current during 3-phase ground fault is also presented. The study in this paper aids in designing the DC link parameters to ensure fast recovery from grid faults. This study also helps in choosing C_d and L_d that lead to lower rotor current, rotor voltage, DC link voltage and current transient peaks to protect the switches of the rotor converter from over-current and over-voltage that occur due to grid faults. The choice of DC link parameters will aid fault ride through (FRT) with any proposed devices such as DVR, STATCOM.

References:

[1] Abdul Salam D., and Riadh A., “Wind energy state of the art: present and future technology advancements”, Renew. Energy Environ. Sustain., 2020, 5, (7), pp 1-8.

[2] Haidi T., Cheddad B., “State of Wind Energy in the World: Evolution, Impacts and Perspectives “, International Journal on “Technical and Physical Problems of Engineering, 2022, 14, (2), pp. 347-352.

[3] Andi Hida, Lorenc Malka, Rajmonda Bualoti, "Wind Power Integration and Challenges in Low Wind Zones. A Study Case: Albania", WSEAS Transactions on Power Systems, 2024, 19, pp. 204-228.

[4] Panda S.; Panda B.; Kumar R.; et al., “Wind Energy Conversion Systems and Technologies: A Summary of the Current State of the Art, 2023 IEEE 3rd International Conference on Sustainable Energy and Future Electric Transportation (SEFET), India, August 2023.

[5] M. Abdelateef Mostafa, Enas A. El-Hay · Mahmoud M. ELkholy, "Recent Trends in Wind Energy Conversion System with Grid Integration Based on Soft Computing Methods: Comprehensive Review, Comparisons and Insights", Archives of Computational Methods in Engineering ,2023, 30, pp. 1439–1478

[6] Saleh M., Eskander M., “ Sizing of Converters Interfacing the Rotor of Wind Driven DFIG to the

Power Grid ", Smart Grid and Renewable Energy journal, 2011, 2, (3), pp. 300-304.
[7] Du C., , Du X., Chenghui T., et al. , "Stability Analysis for DFIG-Based Wind Farm Grid-Connected System Under All Wind Speed Conditions", IEEE Trans. on Industry Applications, 2023, 59, (2), pp. 2430-2445.
[8] Oladapo T. Ibitoye, Moses O. Onibonoje, Joseph O. Dada, Omolayo M. Ikumapayi, Opeyeolu T. Laseinde, "An Enhanced Edge Computing Technique for Detection of Voltage Fluctuation in Grid-tied Renewable Energy", WSEAS Transactions on Power Systems, vol. 19, pp. 338-349, 2024
[9] Musarrat N., Fekih A., Rahman A., et al. , "An Event-Triggered Sliding Mode Control-Based Fault Ride-Through Scheme to Improve the Transient Stability of Wind Energy Systems", IEEE Trans. on Industry Applications, 2024, 60, (1), pp. 876-886.
[10] Donghui S. , Zixuan Z. , Jie R. , et al., "SMES Based Reconfigured Converter Architecture for DFIG to Enhance FRT and Grid Forming Capability", IEEE Trans. on Applied Superconductivity, 2024, 34, (8).
[11] Loulijat A. , Makhad M., Hilali A. , et al. "Enhancing Fault Ride-Through Capacity of DFIG-Based WPs by Adaptive Backstepping Command Using Parametric Estimation in Non-Linear Forward Power Controller Design", IEEE Access, 2024, 12, pp. 58675-58689
[12] AbdelkaderAchar1*, Youcef Djeriri1 , Habib Benbouhenni2 , Ilhami Colak2 , Mihai Oproescu3 & Nicu Bizon3 Self-fltering based on the fault ride-through technique using a robust model predictive control for wind turbine rotor current, Scientific Reports, 2024, 14, article No.1905, pp. 1-46. |
[13] Musarrat M. N., Fekih A.,. Rahman M.A., et al., "A fault ride through scheme to improve the transient stability of wind energy systems," in Proc. IEEE IAS Glob. Conf. Emerg. Technol., 2022, pp. 486–491.
[14] Ulas Karaagac a , Ilhan Kocar b,* , Jean Mahseredjian b , Lijun Cai c , Zahid Javid , " STATCOM integration into a DFIG-based wind park for reactive power compensation and its impact on wind park high voltage ride-through capability", Electric Power Systems Research, 2021, 199, 107368,pp,1-8.
[15] Sanaa M. I. Amer, Mona N. Eskander, "Effect of DC Link Capacitor on the Performance of Wind-Driven Double-Fed Induction Generator", WSEAS Transactions on Power Systems, vol. 19, pp. 44-53, 2024
[16] Amevi Acakpov, Essel Ben Hagan, "A Wind Turbine System Model using a Doubly-Fed Induction Generator (DFIG)", International Journal of Computer Applications, 2014, 90, 15, pp.6-11
[17] Ibrahim M., Nashed M.,Eskander M., "Comparing Methods to Mitigate the Effect of Grid Voltage Sag and Frequency Variation on the Operation of Variable Speed Drives", WSEAS Transaction on Power Systems, 2024, 19, 2, pp. 11-17

Contribution of Individual Authors to the Creation of a Scientific Article (Ghostwriting Policy)

The authors equally contributed in the present research, at all stages from the formulation of the problem to the final findings and solution.

Sources of Funding for Research Presented in a Scientific Article or Scientific Article Itself

No funding was received for conducting this study.

Conflict of Interest

The authors have no conflicts of interest to declare that are relevant to the content of this article.